IEEE Access
Multidisciplinary | Rapid Review | Open Access Journal

Received December 24, 2016, accepted January 23, 2017, date of publication February 14, 2017, date of current version March 15, 2017.

Digital Object Identifier 10.1109/ACCESS.2017.2669209

Natural Walking Reference Generation Based on Double-Link LIPM Gait Planning Algorithm

TZUU-HSENG S. LI, (Member, IEEE), YA-FANG HO, PING-HUAN KUO, YAN-TING YE, AND LI-FAN WU

aiRobots Laboratory, Department of Electrical Engineering, National Cheng Kung University, Tainan 701, Taiwan

Corresponding author: T.-H. S. Li (thsli@mail.ncku.edu.tw)

This work was supported in part by the Ministry of Science and Technology, Taiwan, under Grant MOST 103-2221-E-006-252 and Grant MOST 104-2221-E-006-228-MY2, and in part by the Ministry of Education, Taiwan, within the Aim for the Top University Project through National Cheng Kung University, Tainan, Taiwan.

ABSTRACT In this paper, an enhanced linear inverted pendulum model (LIPM) and a gait planning algorithm are proposed. The LIPM is a widely used concept for gait reference generation, and it provides a simplified model for planning a center of mass trajectory when given a proper zero moment point trajectory. However, one of the assumptions of LIPM is that the legs of the robot are massless, so that the mass of the supporting leg can be neglected for simplification, and it conflicts with the mass distributions of human beings and most humanoid robots. Hence, this paper proposes a double-link LIPM (DLIPM) to eliminate the conflict about mass distribution. In addition, a gait planning algorithm is proposed for natural walking reference generation. In the simulation results, the proposed method is implemented based on a model of a teen-sized humanoid robot named David Junior. The simulation results validate the feasibility and practicability of the proposed method. Moreover, comparisons between conventional LIPM and DLIPM demonstrate the performance of the proposed DLIPM method. Eventually, the proposed method is implemented on David Junior for the weight-lifting event in the 2015 FIRA RoboWorld Cup, an event which David Junior won first place.

INDEX TERMS Biped gait generation, humanoid robots, linear inverted pendulum model (LIPM), zero moment point (ZMP).

I. INTRODUCTION

Humanoid robot is a type of robot which possesses human-like appearance and is able to perform human-like motions. This robot is expected to replace the wheeled robot in certain situations such as environments containing rugged terrain and stairs since the wheeled robot is not able to move freely in such environments. Furthermore, this robot is expected to explore and work on other planets in the future. This requirement has stimulated research associated with stable human-like motion generation, and so stable biped walking [1]–[5] is an essential research topic in this field. Several concepts have been proposed for biped walking, including biological inspiration [6]–[8], Central Pattern Generator (CPG) [9]–[12], model predictive control [13], [14], Zero Moment Point (ZMP) [15]–[20], and Inverted Linear Pendulum Model (LIPM) [21]–[26].

ZMP is the most well-known stability criterion for biped walking, and LIPM provides a simplified model to realize real-time biped walking reference generation. Due to the simplified model, LIPM is easy to implement and might be more suitable for real-time gait planning than other gait planning methods aforementioned. Therefore, many researchers have utilized these two concepts to propose valuable methods for stable biped walking. Erbatur and Kurt [27], [28] proposed a natural reference generation method based on LIPM and moving supporting leg ZMP reference, which was inspired by the human ZMP trajectory. CoM references derived from moving ZMP references were approximated by the Fourier series, and Lanczos sigma factors [29] were employed to smooth the approximated reference and to obtain the desired double support phase [27], [28]. Lee *et al.* [30] presented a real-time modifiable walking pattern generator which is able to dynamically adjust the walking period and foot placements during walking. By construction of feasible regions to determine the nearest feasible motion, the appropriate variation of ZMP was obtained by two closed-form functions. Shin and Kim [31] established energy-efficient gait planning based on LIPM and allowable ZMP region. An online

gait synthesis algorithm generated a complete walking cycle, compromising walking stability and energy efficiency.

The conventional LIPM concept utilized in the aforementioned methods simplifies the model of a robot as a fixed-height mass point with massless legs, so the model is mass-distribution invariant. In terms of implementation, the simplified model makes the walking reference generation efficient because constructing an accurate mathematical model of a robot is difficult and time-consuming, and it has a high computational cost. Thus, LIPM is a widely utilized concept for biped walking. However, one assumption of LIPM, that is the legs of the robot are massless, conflicts with mass distributions of human beings and most biped robots. To comply with this assumption, the mass of legs should be much less than the mass of the upper body. Otherwise, the modeling error will affect the stability strongly. On the other hand, the mass distribution of the robot indeed affects the walking stability, so it should be considered into the model of the robot. Therefore, this paper proposes a double-link linear inverted pendulum model to introduce the mass distribution of the robot into the model. The model proposed in this paper preserves the characteristics of LIPM while providing a human-like walking reference generator.

There have been some literatures associated with multi-link inverted pendulum models. Park *et al.* proposed a gravity compensated inverted pendulum mode (GCIPM) with two masses. One mass is mass of the free leg, namely swing leg, and the other mass is mass of the robot excluding the free leg [32]. Erbatur and Seven [33] proposed one-mass-two-mass switching linear inverted pendulum models, which consider the mass of the swing leg in single support phase. A robot was modeled as a one-mass model in double support phase and as a two-mass model in single support phase. Buschmann *et al.* [34] also considered the swing leg and presented a three-mass inverted pendulum model to reduce the torso oscillations caused by the swing leg. Instead of gait generation, Stephens presented a balance controller with double inverted pendulum model, which allows a robot to maintain an upright posture when it is pushed by a large force [35]. Most of the aforementioned methods considered the minor mass as mass of the swing leg. In contrast, this paper provides another concept for multi-link inverted pendulum model, namely the minor mass of the proposed double-link linear inverted pendulum model is regarded as mass of the supporting leg.

The main contribution of this paper is to propose a double-link linear inverted pendulum model and a gait planning algorithm to generate natural walking patterns. The double-link model eliminates the conflict between the assumption of the conventional LIPM method and the mass distribution of the robot. The mass of the upper body and the mass of the supporting leg are both considered in the double-link model, yet the low computational cost characteristic of the conventional LIPM method is still preserved. Besides, instead of using Fourier series approximation like [28], the analytical solution of CoM motion is derived from a natural ZMP trajectory. Eventually, the proposed gait planning algorithm introduces a complete procedure for generating a natural walking pattern with user-defined parameters. The simulation results validate the feasibility and the practicability of the proposed method and demonstrate performance of the proposed double-link linear inverted pendulum model.

This paper is organized as follows. Section II briefly introduces the concepts of the conventional LIPM. Then, the double-link linear inverted pendulum model is presented and the difference of the conventional LIPM and the proposed DLIPM is mentioned. In Section III, a natural reference generation method and a gait planning algorithm is proposed. Section IV shows the simulation results with a teen-sized humanoid robot named David Junior [36], and the conclusions are depicted in Section V.

II. COM TRAJECTORY WITH DLIPM

In this section, the conventional LIPM is briefly introduced first since the proposed method in this paper is based on this concept. Then, DLIPM is proposed and the difference between DLIPM and conventional LIPM is also described.

A. DYNAMICS OF CONVENTIONAL LIPM

In LIPM theory, the robot model in the single support phase is simplified as an inverted pendulum whose height is fixed at a constant value. There are three basic assumptions in LIPM. First, the mass of the robot concentrates at a point, which is the center of mass (CoM) of the robot. Second, the mass of the supporting leg is assumed to be massless, which can be achieved approximately if the mass of the leg is much less than the mass of the upper body. Third, the CoM is constrained at a constant height z_c. Because of the third assumption, the linear system can be decoupled in the sagittal plane and the lateral plane. Besides, the control torque at the contact point is generally considered to be zero. Hence, the equation of motion of the CoM in sagittal plane and lateral plane is as follows

$$\begin{bmatrix} \ddot{x} \\ \ddot{y} \end{bmatrix} = \frac{g}{z_c} \begin{bmatrix} x \\ y \end{bmatrix} \tag{1}$$

where g is the gravity constant and z_c is the constant height of the CoM. It is noted that in this paper x and y are defined as sagittal direction and lateral direction, respectively.

Considering ZMP theory, which is a well-known criterion for stable biped walking, the relationship between CoM and ZMP is regarded as the most important feature for robot walking. The relationship of CoM and ZMP is acquired through (2), and the most intuitive way to obtain these equations is using torque balance as shown in Fig. 1 so that the contact point satisfies the zero moment condition. Equation (2) displays a torque balance equation in both sagittal

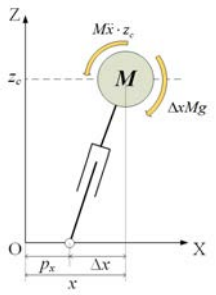

FIGURE 1. Torque balance for LIPM in the sagittal plane.

and lateral planes.

$$\begin{bmatrix}\ddot{x}\\ \ddot{y}\end{bmatrix} = \frac{g}{z_c}\begin{bmatrix}x\\ y\end{bmatrix} - \frac{g}{z_c}\begin{bmatrix}p_x\\ p_y\end{bmatrix} = \omega_n^2\begin{bmatrix}x\\ y\end{bmatrix} - \omega_n^2\begin{bmatrix}p_x\\ p_y\end{bmatrix} \quad (2)$$

where ω_n is defined as $\sqrt{g/z_c}$. p_x and p_y denote the coordinate of ZMP in the sagittal and the lateral planes, respectively.

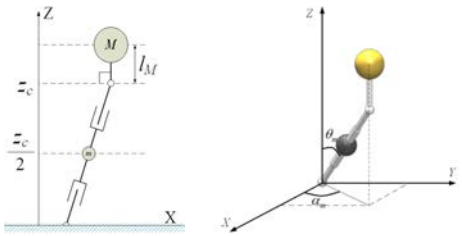

FIGURE 2. Double-link linear inverted pendulum model. (a) 2-D coordinates. (b) 3-D coordinates.

B. DLIPM

Although LIPM can be easily implemented in a real robot at low computational cost due to its linear model, the simplified model is far from the real situation. According to the second assumption, the mass of the supporting leg should be much less than the mass of the body. This assumption brings about a conflict between human mass distribution and robot mass distribution. Moreover, this assumption limits the capability of the robot because a light leg usually means it is thin and weak at the same time. Also, it is difficult for a robot, whose leg is much lighter than the upper body, to execute various tasks such as weight lifting, stair climbing, and jumping. Therefore, the mass of the leg should be considered in the model. Based on this idea, DLIPM is proposed in this paper. There are four assumptions of DLIPM, and the definition of the model is depicted in Fig. 2.

1) The mass M of the upper body and arms is concentrated at one point.
2) The mass m of the supporting leg is concentrated at one point near the middle of the leg.
3) M is always on a fixed height horizontal plane whose height is $z_c + l_M$. Similarly, m is on a fixed height horizontal plane whose height is $z_c/2$.
4) The stick which attaches the mass M is always perpendicular to the horizontal plane.

rm and **rM** are coordinates of mass m and M with respect to the contact point, respectively.

$$\mathbf{r}_m = \begin{bmatrix}r_{mx}\\ r_{my}\\ r_{mz}\end{bmatrix} = \begin{bmatrix}l_m\sin\theta_m\cos\alpha_m\\ l_m\sin\theta_m\sin\alpha_m\\ l_m\cos\theta_m\end{bmatrix} = \begin{bmatrix}\frac{z_c}{2}\tan\theta_m\cos\alpha_m\\ \frac{z_c}{2}\tan\theta_m\sin\alpha_m\\ \frac{z_c}{2}\end{bmatrix} \quad (3)$$

$$\mathbf{r}_M = \begin{bmatrix}r_{Mx}\\ r_{My}\\ r_{Mz}\end{bmatrix} = \begin{bmatrix}2r_{mx}\\ 2r_{my}\\ 2r_{mz}+l_M\end{bmatrix} \quad (4)$$

where l_m is the distance between m and the contact point.

Since r_{mz} is constant, $\dot{r}_{mz}$ is zero. Then, the first order differential equation and second order differential equation of $\mathbf{r}_M$ are as follows

$$\dot{\mathbf{r}}_M = \begin{bmatrix}\dot{r}_{Mx}\\ \dot{r}_{My}\\ \dot{r}_{Mz}\end{bmatrix} = \begin{bmatrix}2\dot{r}_{mx}\\ 2\dot{r}_{my}\\ 2\dot{r}_{mz}\end{bmatrix} = \begin{bmatrix}2\dot{r}_{mx}\\ 2\dot{r}_{my}\\ 0\end{bmatrix} \quad (5)$$

$$\ddot{\mathbf{r}}_M = \begin{bmatrix}\ddot{r}_{Mx}\\ \ddot{r}_{My}\\ \ddot{r}_{Mz}\end{bmatrix} = \begin{bmatrix}2\ddot{r}_{mx}\\ 2\ddot{r}_{my}\\ 0\end{bmatrix}. \quad (6)$$

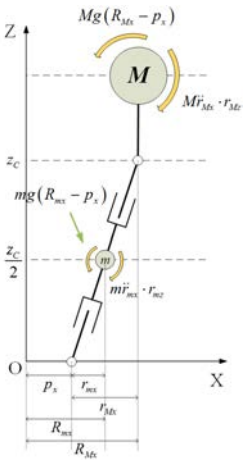

FIGURE 3. Torque balance for DLIPM in the sagittal plane.

In order to derive the relationship between ZMP and CoM, the torque balance is applied. The x-direction torque balance is demonstrated in Fig. 3 and (7). R_{Mx} and R_{mx} are x-coordinate of mass M and mass m with respect to the world coordinate, respectively.

$$Mg(R_{Mx}-p_x) + mg(R_{mx}-p_x) = M\ddot{r}_{Mx}\cdot r_{Mz} + m\ddot{r}_{mx}\cdot r_{mz} \quad (7)$$

As shown in Fig. 3, R_{Mx} and R_{mx} can be expressed as follows

$$R_{Mx} = p_x + r_{Mx} = p_x + 2r_{mx} \quad (8)$$

$$R_{mx} = p_x + r_{mx} = \frac{1}{2}p_x + \frac{1}{2}R_{Mx}. \tag{9}$$

After substituting (3)-(6) and (9) into (7), the torque balance equations become as follows

$$\ddot{R}_{Mx}\left(Mz_c + \frac{1}{4}mz_c + Ml_M\right) = \left(M + \frac{1}{2}m\right)gR_{Mx} - \left(M + \frac{1}{2}m\right)gp_x \tag{10}$$

where $\ddot{R}_{Mx} = \ddot{r}_{Mx}$.

Defining $\tilde{\omega}_n = \sqrt{(M + m/2)g/(Mz_c + Ml_M + mz_c/4)}$, (10) can be rewritten as follows

$$\ddot{R}_{Mx} = \tilde{\omega}_n^2 R_{Mx} - \tilde{\omega}_n^2 p_x. \tag{11}$$

Similarly, the y-direction torque balance can be derived in the same way, so the dynamics of mass M can be expressed as (12).

$$\begin{bmatrix} \ddot{R}_{Mx} \\ \ddot{R}_{My} \end{bmatrix} = \tilde{\omega}_n^2 \begin{bmatrix} R_{Mx} \\ R_{My} \end{bmatrix} - \tilde{\omega}_n^2 \begin{bmatrix} p_x \\ p_y \end{bmatrix} \tag{12}$$

Since the mass M is always perpendicular to the horizontal plane, R_{Mx} and R_{My} also denote the x-coordinate and the y-coordinate of CoM, respectively. Therefore, the equation of motion of the CoM with the proposed DLIPM method is:

$$\begin{bmatrix} \ddot{x} \\ \ddot{y} \end{bmatrix} = \tilde{\omega}_n^2 \begin{bmatrix} x \\ y \end{bmatrix} - \tilde{\omega}_n^2 \begin{bmatrix} p_x \\ p_y \end{bmatrix}. \tag{13}$$

with

$$\tilde{\omega}_n = \sqrt{(M + m/2)g/(Mz_c + Ml_M + mz_c/4)}.$$

It can be seen that the formula of the CoM trajectory obtained from DLIPM is very close to that of conventional LIPM derived in [28], whereas the definition of $\tilde{\omega}_n$ of DLIPM is quite different from that of conventional LIPM. ω_n of conventional LIPM, which is defined as $\sqrt{g/z_c}$, is only related to the gravity constant and the height of CoM. It means that the CoM trajectory of conventional LIPM is completely independent of the mass distribution of the robot. However, it is obvious that the mass distribution of the robot will strongly affect the stability of the gait patterns. Hence, the mass-distribution-independent characteristic of conventional LIPM might be regarded as a defect. In contrast, the mass distribution is considered in DLIPM. Although the computational cost of ω_n of DLIPM is slightly higher than that of conventional LIPM, time cost of DLIPM still can be regarded the same as time cost of conventional LIPM since M, m, and l_M are constant during walking. Considering the mass distribution makes the model more realistic. The experiment results will verify this improvement and demonstrate that the gait pattern generated by DLIPM is better than the conventional LIPM.

III. NATURAL REFERENCE GENERATION

A. CoM TRAJECTORIES WITH NATURAL ZMP REFERENCES

Since the relationship between CoM and ZMP of DLIPM is formulated in the previous section, the CoM reference trajectory can be derived with (13) though a given ZMP trajectory. Applying Laplace transformation, the analytical solutions of (13), namely the sagittal CoM motion and the lateral CoM motion, are obtained as follows

$$\begin{bmatrix} x(t) \\ v_x(t) \end{bmatrix} = \begin{bmatrix} C(t) & \frac{1}{\tilde{\omega}_n}S(t) \\ \tilde{\omega}_n S(t) & C(t) \end{bmatrix} \begin{bmatrix} x_0 \\ v_{x0} \end{bmatrix} + \begin{bmatrix} \bar{p}(t) \\ \frac{d}{dt}\bar{p}(t) \end{bmatrix} \tag{14}$$

$$\begin{bmatrix} y(t) \\ v_y(t) \end{bmatrix} = \begin{bmatrix} C(t) & \frac{1}{\tilde{\omega}_n}S(t) \\ \tilde{\omega}_n S(t) & C(t) \end{bmatrix} \begin{bmatrix} y_0 \\ v_{y0} \end{bmatrix} + \begin{bmatrix} \bar{q}(t) \\ \frac{d}{dt}\bar{q}(t) \end{bmatrix} \tag{15}$$

with

$$\bar{p}(t) = \mathcal{L}^{-1}\left(\frac{-\tilde{\omega}_n^2}{s^2 - \tilde{\omega}_n^2}P(s)\right) \text{ and } \bar{q}(t) = \mathcal{L}^{-1}\left(\frac{-\tilde{\omega}_n^2}{s^2 - \tilde{\omega}_n^2}Q(s)\right)$$

where (x_0, v_{x0}) and (y_0, v_{y0}) denote initial position and initial velocity of CoM in sagittal and lateral planes, respectively. $C(t)$ and $S(t)$ are defined as $\cosh(\tilde{\omega}_n t)$ and $\sinh(\tilde{\omega}_n t)$, respectively. $P(s)$ and $Q(s)$ are the respective Laplace transforms of ZMP trajectories $p(t)$ and $q(t)$. $\mathcal{L}^{-1}(\cdot)$ denotes inverse Laplace transform.

Then, substituting a desired ZMP trajectory into the second term of the right hand side of (14) and (15), the CoM reference motion can be obtained. However, there is a problem when using (14) and (15) to generate a CoM reference trajectory. When t becomes much greater than zero, the values of $C(t)$ and $S(t)$ tend to infinity. Thus, it is necessary to generate CoM reference trajectory step by step with given boundary conditions for each step. Hereinafter, derivation of the CoM reference trajectory will be discussed for a single step.

Inspired by [28], a natural ZMP trajectory is considered for moving forward slightly during single support phase. Thus, the ZMP trajectory with considering double support phase for a single step is defined as follows

$$\begin{cases} p_n(t) = (A_n - d_{1,n} + \dfrac{d_{1,n} - a_n}{k_v T}t)\,[u(t) - u(t - t_1)] \\ \quad + \left[(\dfrac{2a_n}{t_2 - t_1})(t - t_1) + A_n - a_n\right][u(t - t_1) - u(t - t_2)] \\ \quad + \left[A_n + a_n + \dfrac{d_{2,n} - a_n}{k_v T}(t - t_2)\right]u(t - t_2) \\ q_n(t) = \dfrac{B_n}{k_v T}t\,[u(t) - u(t - t_1)] \\ \quad + B_n\,[u(t - t_1) - u(t - t_2)] \\ \quad + \left[B_n - \dfrac{B_n}{k_v T}(t - t_2)\right]u(t - t_2) \end{cases} \tag{16}$$

where $u(\cdot)$ denotes unit step function and $t \in (0, T]$. T denotes period of a step, which is half of walking period. Subscript n denotes the n-th step. A denotes the sagittal amplitude, B denotes the lateral amplitude, and a denotes half of the distance that ZMP moves forward during a single support phase. Virtual DSP scale k_v is defined to make the velocity of CoM smoother at boundaries, and does not affect the actual period of DSP. t_1 is $k_v T$ and t_2 is $(1 - k_v)T$. It is noted that $(A - d_1, A + d_2)$ is defined as the initial and the final position

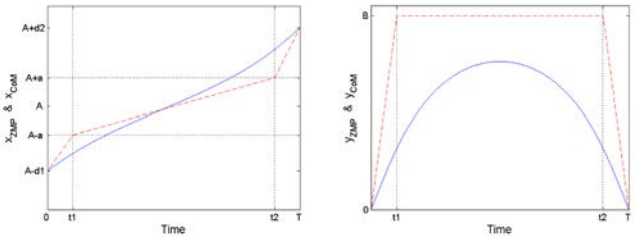

(a) (b)

FIGURE 4. Natural ZMP and CoM trajectory for a single step. CoM trajectory is shown on a solid line, and ZMP is shown on a dashed line. (a) In sagittal plane. (b) In lateral plane.

of CoM and ZMP in the sagittal plane, and (0, 0) is defined as the initial and the final position of CoM and ZMP in the lateral plane. For simplicity, the subscript n will be omitted when no ambiguity arises. Natural ZMP and CoM trajectory for a single step is depicted as Fig. 4.

Substituting the Laplace transform of $p(t)$ into (14) and defining $L_1 = A - d_1$, $K_1 = (d_1 - a)/kT$, $L_2 = A - a - 2at_1/(t_2 - t_1)$, $K_2 = 2a/(t_2 - t_1)$, $L_3 = A + a - (d_2 - a)t_2/kT$, $K_2 = (d_2 - a)/kT$, then the CoM reference trajectory in the sagittal plane can be obtained as

$$x(t) = x_0 C(t) + \frac{v_{x0}}{\tilde{\omega}_n} S(t) + x_1(t) + x_2(t) + x_3(t) \quad (17)$$

with

$$\begin{aligned}
x_1(t) &= L_1 [1 - C(t)] u(t) + K_1 \left[t - \frac{1}{\tilde{\omega}_n} S(t) \right] u(t) \\
x_2(t) &= (L_2 - L_1) [1 - C(t - t_1)] u(t - t_1) \\
&\quad + (K_2 - K_1) \left[t - t_1 C(t - t_1) - \frac{1}{\tilde{\omega}_n} S(t - t_1) \right] \\
&\quad \times u(t - t_1) \\
x_3(t) &= (L_3 - L_2) [1 - C(t - t_2)] u(t - t_2) \\
&\quad + (K_3 - K_2) \left[t - t_2 C(t - t_2) - \frac{1}{\tilde{\omega}_n} S(t - t_2) \right] \\
&\quad \times u(t - t_2).
\end{aligned}$$

Now the only one unknown variable of (17) is the initial velocity v_{x0}. To determine v_{x0}, substitute the boundary conditions, namely the initial position x_0 (whose value is $A - d_1$) and the final position x_{final} (whose value is $A + d_2$), into (17), then v_{x0} can be obtained by the following equations.

$$\begin{aligned}
x_{\text{final}} &= x(T) = x_0 C(T) + \frac{v_{x0}}{\tilde{\omega}_n} S(T) + x_1(T) + x_2(T) + x_3(T) \\
v_{x0} &= \frac{\tilde{\omega}_n}{S(T)} [x_{\text{final}} - x_0 C(T) - x_1(T) - x_2(T) - x_3(T)] \\
v_{x0} &= \frac{\tilde{\omega}_n}{S(T)} [A + d_2 - (A - d_1) C(T) \\
&\quad - x_1(T) - x_2(T) - x_3(T)] \quad (18)
\end{aligned}$$

Similarly, substituting the Laplace transform of $q(t)$ into (15), then the CoM reference trajectory in the lateral plane can be obtained as

$$y(t) = y_0 C(t) + \frac{v_{y0}}{\tilde{\omega}_n} S(t) + y_1(t) + y_2(t) + y_3(t) \quad (19)$$

with

$$\begin{aligned}
y_1(t) &= \frac{B}{kT} \left[t - \frac{1}{\tilde{\omega}_n} S(t) \right] u(t) \\
y_2(t) &= B [1 - C(t - t_1)] u(t - t_1) \\
&\quad - \frac{B}{kT} \left[t - t_1 C(t - t_1) - \frac{1}{\tilde{\omega}_n} S(t - t_1) \right] u(t - t_1) \\
y_3(t) &= \frac{Bt_2}{kT} [1 - C(t - t_2)] u(t - t_2) \\
&\quad - \frac{Bt}{kT} \left[t - t_2 C(t - t_2) - \frac{1}{\tilde{\omega}_n} S(t - t_2) \right] u(t - t_2).
\end{aligned}$$

To determine v_{y0}, substitute the boundary conditions, namely the initial position y_0 (whose value is 0) and the final position y_{final} (whose value is 0), into (19), then v_{y0} can be obtained by the following equations.

$$\begin{aligned}
y_{\text{final}} &= y(T) = y_0 C(T) + \frac{v_{y0}}{\tilde{\omega}_n} S(T) + y_1(T) + y_2(T) + y_3(T) \\
v_{y0} &= -\frac{\tilde{\omega}_n}{S(T)} [y_1(T) + y_2(T) + y_3(T)] \quad (20)
\end{aligned}$$

In short, given amplitudes of ZMP (A, B, a), boundary conditions (d_1, d_2), and virtual DSP scale k_v, initial velocities v_{x0} and v_{y0} can be determined by (18) and (20), respectively. Then, the CoM reference trajectory in the sagittal and the lateral plane for a single step can be obtained by (17) and (19).

B. GAIT PLANNING ALGORITHM

In the aforementioned section, the derivation of the CoM reference trajectory for a single step is presented. As the parameters of each step, namely $\{A_n, B_n, a_n, d_{1,n}, d_{2,n}, k_{v,n}\}$, are determined, a complete gait can be acquired. Thus, this section will propose a gait planning algorithm for generating a complete gait. To generate a gait with the goal distance D and the goal speed V, the gait planning algorithm consists of the following steps:

1) Determine the number of steps N, then the period T is determined as $T = D/(NV)$.
2) Assume that the amplitude increment of the first step S_1 is zero and the amplitude increment for the other steps are identical. Thus, $S_1 = 0$ and $S_n = D/(N - 1)$ for $n \in \{2, ..., N\}$. Then, the sagittal amplitude for the n-th step is

$$A_n = \sum_{i=1}^{n} S_i \text{ for n} \in \{1, 2, ..., N\}. \quad (21)$$

3) To accelerate at the first step and decelerate at the final step in the sagittal plane, $d_{1,1}$, which is d_1 of the first step and $d_{2,N}$, which is d_2 of the final step, are assigned zero. In addition, since the initial position of a step must be same as the final position of its previous step, we can know

$$d_{2,n} = \frac{A_{n+1} - A_n}{2} \text{ for n} \in \{1, ..., N-1\} \quad (22)$$

$$d_{1,n+1} = d_{2,n} \text{ for n} \in \{1, ..., N-1\}. \quad (23)$$

4) B_n, a_n, and $k_{v,n}$ are user-defined parameters. Generally, B_n is half of step width, and step width of each step is identical. a_n is relatively small compared to A_n. In this paper, a_n is chosen as 0.01 A_n as A_n is greater than zero; otherwise, a_n is zero. $k_{v,n}$ of each step is identical, and $k_{v,n}$ is chosen as 0.1 in this paper.
5) Since $\{A_n, B_n, a_n, d_{1,n}, d_{2,n}, k_v, n\}$ for n $\in \{1, 2, ..., N\}$ are determined, the initial condition for each step can be calculated by (18) and (20). Then, the CoM reference trajectory for each step can be obtained by (17) and (19). Thus, the complete CoM reference trajectory in the sagittal and the lateral plane are as follows

$$x(t) = \sum_{n=1}^{N} x_n(t-(n-1)T) \times [u(t-(n-1)T) - u(t-nT)] \quad (24)$$

$$y(t) = \sum_{n=1}^{N} y_n(t-(n-1)T) \times [u(t-(n-1)T) - u(t-nT)]. \quad (25)$$

6) Determine step height and calculate the foot trajectories with respect to the world coordinate system. Assume that the first swing leg is the right leg. Then, the stride length of both feet for each step are

$$L_{r,n} = \begin{cases} A_{n+1} - A_{n-1}, \\ \quad \text{for } n = \{2i-1 \,|\, \forall i \in \mathbb{N}^+, 2i-1 \le N\} \\ 0, \quad \text{for } n = \{2i \,|\, \forall i \in \mathbb{N}^+, 2i \le N\} \end{cases} \quad (26)$$

$$L_{l,n} = \begin{cases} 0, \quad \text{for } n = \{2i-1 \,|\, \forall i \in \mathbb{N}^+, 2i-1 \le N\} \\ A_{n+1} - A_{n-1}, \\ \quad \text{for } n = \{2i \,|\, \forall i \in \mathbb{N}^+, 2i \le N\} \end{cases} \quad (27)$$

where A_0 is defined as zero and A_{N+1} is defined as A_N. Subscript r and l denotes the right foot and the left foot, respectively. It is noted that A_0 and A_{N+1} are virtual amplitudes for calculating step length, and are not utilized in (21).

The foot trajectory generation can be divided into two parts according to the support phase. In the double support phase, both feet stay at fixed points. In the single support phase, the supporting foot stays at the fixed point as well, and the swing foot trajectory is acquired by using a rolling cycle [11]. Then, the foot trajectories with respect to the world coordinate system are

$$footx_{j,n}(t) = \begin{cases} 0, & \text{if } t \le t_1 \\ \frac{L_{j,n}}{2\pi}(\theta - \sin\theta), & \text{if } t_1 < t \le t_2 \\ L_{j,n}, & \text{otherwise} \end{cases} \quad (28)$$

$$footy_{j,n}(t) = 0 \quad (29)$$

$$footz_{j,n}(t) = \begin{cases} \frac{H}{2}(1-\cos\theta), & \text{for } t_1 < t \le t_2 \\ 0, & \text{otherwise} \end{cases} \quad (30)$$

where t_1 is kT and t_2 is $(1-k)T$, $\theta = 2\pi(t-t_1)/(t_2-t_1)$, $t \in (0, T]$ and $j \in \{r, l\}$. The period of DSP is defined by actual DSP scale k, and $k \in (0, 0.25]$ theoretically. Thus, the period of DSP T_{DSP} is $2kT$ and the period of SSP T_{SSP} is $(1-2k)T$. H denotes step height and is also a user-defined parameter.

Since the foot trajectories for each step are known, the complete foot trajectories can be obtained as follows.

$$\begin{cases} footx_j(t) = \sum_{n=1}^{N} \left[O_{j,n} + footx_{j,n}(t-(n-1)T)\right] U(t) \\ footy_j(t) = 0 \\ footz_j = \sum_{n=1}^{N} footz_{j,n}(t-(n-1)T)U(t) \end{cases} \quad (31)$$

with

$$O_{j,1} = 0, \quad O_{j,n} = \sum_{m=1}^{n-1} L_{j,m} \text{ for } n \in \{2, \ldots, N\}$$
$$U(t) = u(t-(n-1)T) - u(t-nT)$$

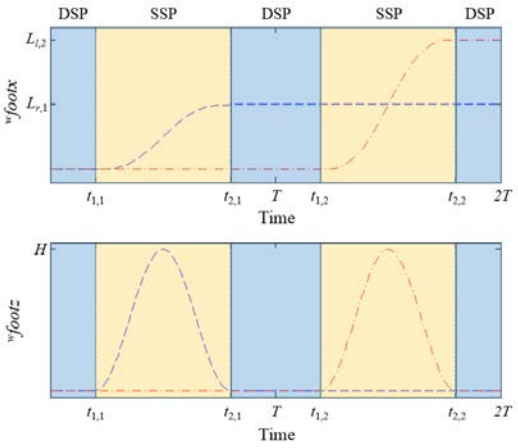

FIGURE 5. Foot trajectory with respect to the world coordinate system. The right foot trajectory is shown on a dashed line, and the left foot trajectory is shown on a dash-dot line.

Fig. 5 shows foot trajectories with two steps. The right foot trajectory is shown on a dashed line, and the left foot trajectory is shown on a dash-dot line. It can be seen that when one foot steps forward within a SSP, the other foot stays at a fixed point.

7) Calculate the foot trajectories with respect to the joint coordinate system ${}^h\mathbf{foot}_j = [{}^h footx_j, {}^h footy_j, {}^h footz_j]^{\mathrm{T}}$ as follows

$${}^h\mathbf{foot}_j = {}^w\mathbf{foot}_j - {}^w\mathbf{CoM} \text{ for } j \in \{r, l\} \quad (32)$$

where ${}^{w}\mathbf{foot}_j = [footx_j, footy_j, footz_j]^{\mathrm{T}}$ and ${}^{w}\mathbf{CoM} = [x, y, z_c]^{\mathrm{T}}$. It is noted that ${}^{h}\mathbf{foot}_j$ should satisfy physical constraints of kinematics of the robot.

8) Finally, apply inverse kinematics.

IV. SIMULATION AND EXPERIMENT RESULTS

To verify the performance of the proposed method, a simulation study was carried out on the Webots simulator [37]. Both the proposed DLIPM method and the conventional LIPM method were implemented to generate gait patterns in the simulator for comparison. In addition, in the simulation study, there were three different cases studied for comparison in terms of robot mass distribution so that the enhancement of the proposed DLIPM method, which takes into account the mass distribution, can be validated.

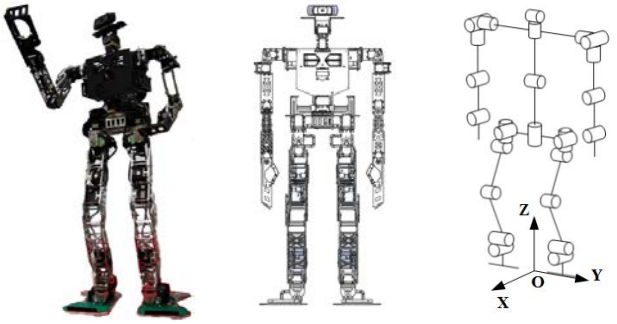

(a) (b) (c)

FIGURE 6. David Junior. (a) Real picture. (b) Structural appearance. (c) Joint configuration.

TABLE 1. Mass distribution for three cases (unit: kg).

	Case 1	Case 2	Case 3
Head	0.426	0.426	0.426
Trunk	2.944	2.944	6.944
Upper Arm	0.52	0.52	0.52
Lower Arm	0.275	0.275	0.275
Thigh	0.59	1.59	0.59
Calf	0.747	1.747	0.747
Sole	1	1	1
Total	9.634	13.634	13.634
Upper-body	4.96	4.96	8.96
Single leg	2.337	4.337	2.337
Ratio of upper-body to leg	2.1224	1.1436	3.834

In the first case, the robot model in the simulator was built based on a teen-sized humanoid robot named David Junior as shown in Fig. 6, which is the first-generation teen-sized humanoid robot from the aiRobots laboratory. David Junior is 96 cm tall, weighs about 9.6 kg, and consists of 26 DOFs driven by servo motors. Each joint is driven by one motor, except for the hip roll joint and the ankle roll joint, which are driven by two motors. Case 1 in Table 1 lists the mass of each part of David Junior. The mass distribution of the robot in the first case was modeled according to the actual mass distribution of David Junior. It can be seen that in the first case, the ratio of the upper body to the supporting leg was approximately 2. The model of David Junior in the simulator is shown in Fig. 7.

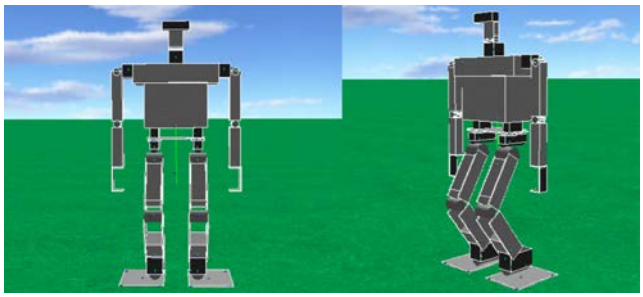

FIGURE 7. Model of David Junior in the simulator.

In the second case, the mass of the thigh and calf were increased to 1.59 kg and 1.747 kg, respectively. Thus, the ratio of upper body to the supporting leg in the second case was approximately 1. In the third case, the mass of the trunk was increased to 6.944 kg. Thus, the mass of the upper body became 8.96 kg, and the ratio of the upper body to the supporting leg in the third case was approximately 4. In summary, these three cases illustrate three different mass distributions of a robot: normal mass distribution, lower body-to-leg ratio, and higher body-to-leg ratio.

A. COMPARISON BETWEEN CONVENTIONAL LIPM AND DLIPM FOR WALKING WITH NORMAL MASS DISTRIBUTION

The gait pattern generated by using the proposed DLIPM method was performed for a comparison with the gait pattern generated by using conventional LIPM. While the robot walked with normal mass distribution, which means the robot walked without any additional weight on the legs or the trunk, z_c was 0.3896 m height and l_M was 0.2099 m. M and m were 4.96 kg and 2.337 kg, respectively. T was set at 0.6 s and the virtual DSP ratio k_v was set at 0.1. We found that the CoM trajectory tended to a straight line as k_v increased, so k_v should be a relatively small value than k. In addition, k was set at 0.22, so $\mathrm{T_{DSP}}$ and $\mathrm{T_{SSP}}$ were 0.264 s and 0.336 s, respectively.

The amplitude increment for each step S_n except for the first steps was set at 8 cm, and the gait pattern contained 16 steps. Therefore, $S = [0, 8, 8, \ldots, 8]$ cm. The magnitude of B_n for each step was set at 11.8 cm, and a_n was set at $0.01A_n$. H was set at 3 cm. Thus, the robot walked with 16 steps in this experiment; the desired goal distance and the average velocity would be 1.2 m and 0.125 m/s, respectively.

With the above-mentioned parameters, the gait patterns generated by the proposed double-link LIPM method and the conventional LIPM method were performed in the simulator. The resulting ZMP and CoM trajectories of both methods are shown in Fig. 8 and Fig. 9, respectively. In Fig. 8, DLIPM denotes the measured ZMP trajectory of the proposed DLIPM method, and SLIPM denotes that of the conventional LIPM method, which consists of a single-link. The dotted lines in

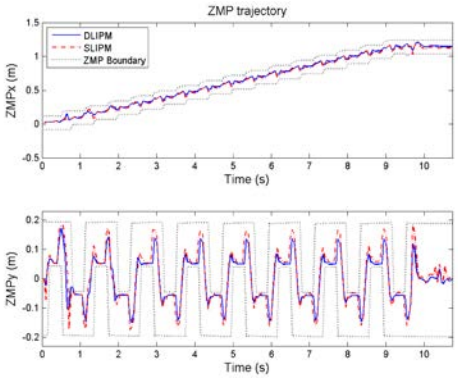

FIGURE 8. The resulting ZMP trajectories of the first case (Normal mass distribution).

Fig. 8 denote ZMP boundaries for stable walking. It can be seen that ZMP vibration of SLIPM was larger than that of DLIPM, especially at 0.7 s and 9.6 s, namely the first step and the last step. This means that the robot accelerated and decelerated more stably when walking with the DLIPM gait pattern.

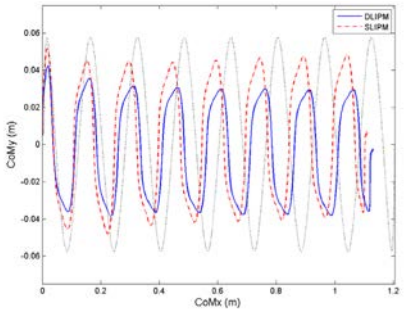

FIGURE 9. The resulting CoM trajectories of the first case (Normal mass distribution).

Fig. 9 shows the resulting CoM trajectories of both methods; the dotted line denotes the desired CoM trajectory. It can be seen that the CoM trajectories of both methods were similar to the desired CoM trajectory, but the walking distances of both methods were less than the desired walking distance. In addition, the resulting CoM trajectory of SLIPM moved toward the left slightly during walking. In contrast, the resulting CoM trajectory of DLIPM showed that the robot could walk straight while walking by using the DLIPM gait pattern.

B. COMPARISON BETWEEN CONVENTIONAL LIPM AND DLIPM FOR WALKING WITH LOWER BODY-TO-LEG RATIO

In the second case, gait pattern parameters were set the same as in the first case except z_c, l_M, M, and m, since they are related to mass distribution. Thus, z_c was 0.3725 m and l_M was 0.2266 m. M and m were 4.96 kg and 4.337 kg, respectively. The resulting ZMP and CoM trajectories of both methods are shown in Fig. 10 and Fig. 11, respectively. Although the ZMP vibration of DLIPM was larger than that of

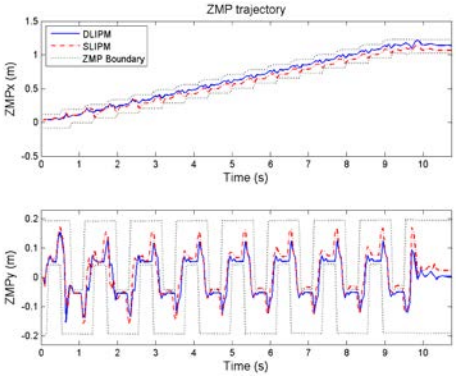

FIGURE 10. The resulting ZMP trajectories of the second case (Lower body-to-leg ratio).

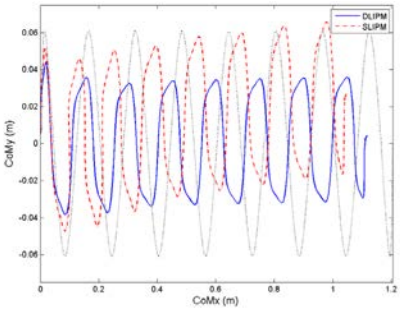

FIGURE 11. The resulting CoM trajectories of the second case (Lower body-to-leg ratio).

SLIPM in the first step, the average ZMP vibration of DLIPM was still lower than in SLIPM. Moreover, Fig. 11 shows that the robot could not walk straight with the SLIPM gait pattern, and the side offset after walking was nearly 0.24 m. In contrast, the side offset of the DLIPM gait pattern was only 0.0023 m.

C. COMPARISON BETWEEN CONVENTIONAL LIPM AND DLIPM FOR WALKING WITH HIGHER BODY-TO-LEG RATIO

Similarly, the gait pattern parameters of the third case were set the same as in the first case except for the parameters related to mass distribution. In the third case, z_c was 0.4324 m and l_M was 0.1384 m. M and m were 8.96 kg and 2.337 kg, respectively. The resulting ZMP and CoM trajectories of both methods are shown in Fig. 12 and Fig. 13, respectively. In the third case, the resulting trajectories of both methods are quite similar, but the amplitude of DLIPM was still less than that of SLIPM. When the height of CoM, namely z_c, was increased, a smaller amplitude of CoMy was beneficial to maintain walking stability.

The simulation results for the three cases are listed in Table 2, which are SAE, actual walking distance, and side offset. SAE denotes the sum of absolute error between the center of the support polygon and the actual ZMP. Actual walking distance and side offset are the final positions of CoM with respect to the x-axis and y-axis, respectively.

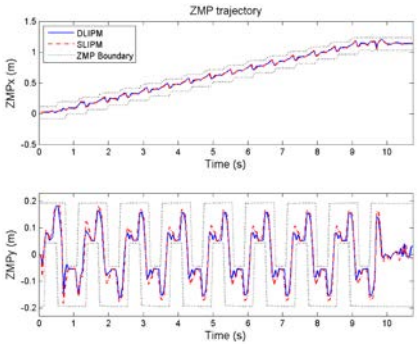

FIGURE 12. The resulting ZMP trajectories of the third case (Higher body-to-leg ratio).

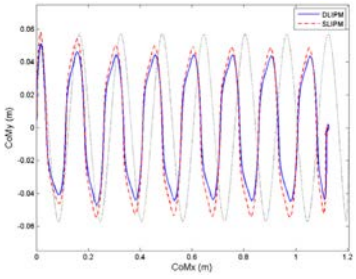

FIGURE 13. The resulting CoM trajectories of the third case (Higher body-to-leg ratio).

TABLE 2. Simulation results for the three cases (uint: m).

		Case 1	Case 2	Case 3
DLIPM	SAE of ZMP_x	4.9575	6.7381	5.0306
	SAE of ZMP_y	14.1111	13.2357	14.4199
	Walking distance	1.1301	1.1178	1.1270
	Side offset	-0.0050	0.0023	-0.0023
SLIPM	SAE of ZMP_x	5.7910	7.8870	5.6433
	SAE of ZMP_y	14.5923	12.1886	14.6836
	Walking distance	1.1105	1.0466	1.1242
	Side offset	0.0041	0.0239	-0.0038

D. EXPERIMENTAL RESULTS

The proposed DLIPM method is implemented on David Junior for the weight-lifting event at the FIRA RoboWorld Cup, which is a well-known international robot competition. In the weight-lifting event, the robot should walk carrying a load on its head to verify its walking stability. The load is a wooden bar with 20 CDs attached on each side like a barbell, and the whole bar weighs 0.719 kg.

Since carrying a load while walking will change the mass distribution of the robot, this event is sufficient to demonstrate the performance of the proposed method. Fig. 14 (refer to supplementary video 1) gives a snapshot of David Junior in the weight-lifting event at the 2015 FIRA RoboWorld Cup. In this event, it has been validated that David Junior is able to walk straight with an additional load on its head. Also,

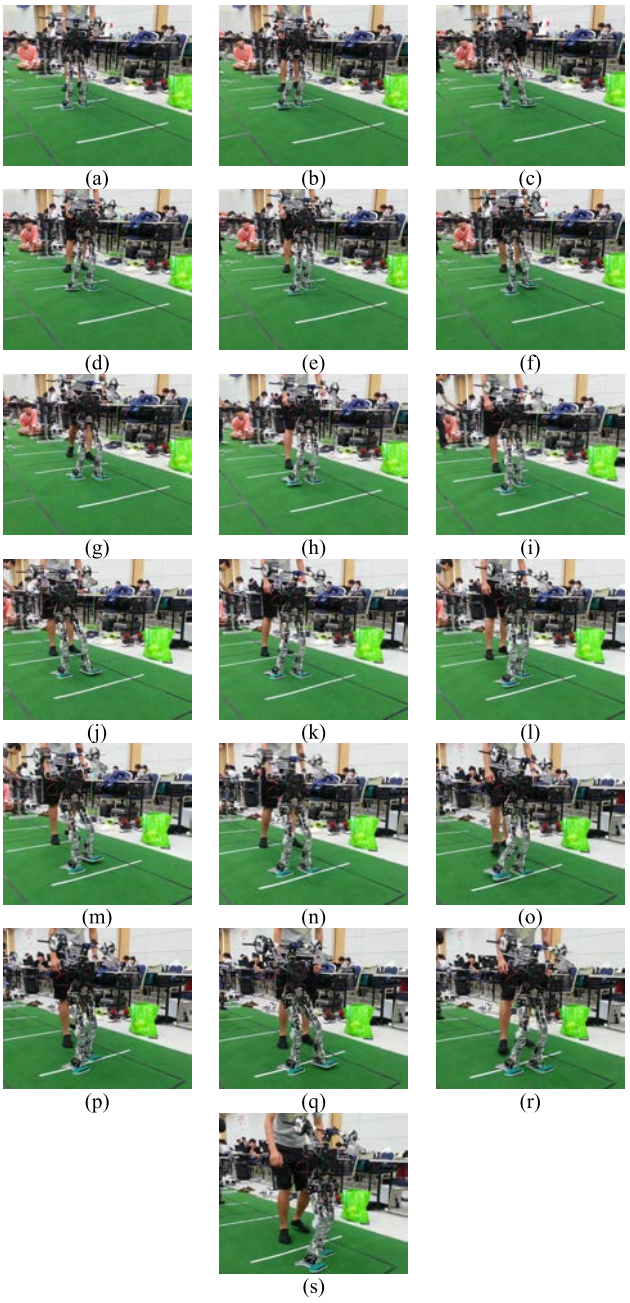

FIGURE 14. Snapshot of weight-lifting event in 2015 FIRA RoboWorld Cup.

David Junior won first place in the weight-lifting event at the 2015 FIRA RoboWorld Cup. Thus, the performance of the proposed DLIPM method is also validated.

V. CONCLUSIONS

In this paper, a double-link linear inverted pendulum model (DLIPM) is proposed to eliminate the conflicting assumption about the conventional linear inverted pendulum model. Thus, the mass distribution of the robot can be taken into account the model while still preserving the easy-to-implement feature of the conventional linear inverted pendulum model. In addition, a gait planning algorithm is proposed

to generate a natural walking reference for the proposed DLIPM method. The simulation results verify the feasibility and the practicability of the proposed method. Moreover, the comparisons of three different mass distributions prove that the performance of the proposed DLIPM walking reference is better than that of the conventional LIPM method in some cases, especially in the first and second cases. Furthermore, in the weight lifting event at the 2015 FIRA RoboWorld Cup, David Junior walked with the gait pattern generated by the proposed method while carrying an additional load on its head and won first place in the weight lifting event. Thus, the performance of the proposed method has also been validated in a real experiment.

REFERENCES

[1] D. J. Braun and M. Goldfarb, "A control approach for actuated dynamic walking in biped robots," *IEEE Trans. Robot.*, vol. 25, no. 6, pp. 1292–1303, Dec. 2009.

[2] Y.-T. Su, K.-Y. Chong, and T.-H. S. Li, "Design and implementation of fuzzy policy gradient gait learning method for walking pattern generation of humanoid robots," *Int. J. Fuzzy Syst.*, vol. 13, no. 4, pp. 369–382, Dec. 2011.

[3] T.-H. S. Li, Y.-T. Su, S.-W. Lai, and J.-J. Hu, "Walking motion generation, synthesis, and control for biped robot by using PGRL, LPI, and fuzzy logic," *IEEE Trans. Syst., Man, Cybern. B, Cybern.*, vol. 41, no. 3, pp. 736–748, Jun. 2011.

[4] P.-H. Kuo, Y.-F. Ho, K.-F. Lee, L.-H. Tai, and T.-H. S. Li, "Development of humanoid robot simulator for gait learning by using particle swarm optimization," in *Proc. IEEE Int. Conf. Syst., Man, Cybern. (SMC)*, Oct. 2013, pp. 2683–2688.

[5] D. J. Braun, J. E. Mitchell, and M. Goldfarb, "Actuated dynamic walking in a seven-link biped robot," *IEEE/ASME Trans. Mechatronics*, vol. 17, no. 1, pp. 147–156, Feb. 2012.

[6] J. Morimoto, G. Endo, J. Nakanishi, and G. Cheng, "A biologically inspired biped locomotion strategy for humanoid robots: Modulation of sinusoidal patterns by a coupled oscillator model," *IEEE Trans. Robot.*, vol. 24, no. 1, pp. 185–191, Feb. 2008.

[7] T. Zielińska, "Biological inspiration used for robots motion synthesis," *J. Physiol.-Paris*, vol. 103, nos. 3–5, pp. 133–140, May/Sep. 2009.

[8] A. A. Saputra, J. Botzheim, I. A. Sulistijono, and N. Kubota, "Biologically inspired control system for 3-D locomotion of a humanoid biped robot," *IEEE Trans. Syst., Man, Cybern. Syst.*, vol. 46, no. 7, pp. 898–911, Jul. 2016.

[9] G. Taga, Y. Yamaguchi, and H. Shimizu, "Self-organized control of bipedal locomotion by neural oscillators in unpredictable environment," *Biol. Cybern.*, vol. 65, no. 3, pp. 147–159, Jul. 1991.

[10] G. Endo, J. Morimoto, T. Matsubara, J. Nakanishi, and G. Cheng, "Learning CPG-based biped locomotion with a policy gradient method: Application to a humanoid robot," *Int. J. Robot. Res.*, vol. 27, no. 2, pp. 213–228, 2008.

[11] C. Liu, D. Wang, and Q. Chen, "Central pattern generator inspired control for adaptive walking of biped robots," *IEEE Trans. Syst., Man, Cybern., Syst.*, vol. 43, no. 5, pp. 1206–1215, Sep. 2013.

[12] T.-H. S. Li, P.-H. Kuo, Y.-F. Ho, M.-C. Kao, and L.-H. Tai, "A biped gait learning algorithm for humanoid robots based on environmental impact assessed artificial bee colony," *IEEE Access*, vol. 3, pp. 13–26, 2015.

[13] R. C. Luo and C. C. Chen, "Biped walking trajectory generator based on three-mass with angular momentum model using model predictive control," *IEEE Trans. Ind. Electron.*, vol. 63, no. 1, pp. 268–276, Jan. 2016.

[14] M. Naveau, M. Kudruss, O. Stasse, C. Kirches, K. Mombaur, and P. Souères, "A reactive walking pattern generator based on nonlinear model predictive control," *IEEE Robot. Autom. Lett.*, vol. 2, no. 1, pp. 10–17, Jan. 2017.

[15] E. Taşkiran, M. Yilmaz, Ö. Koca, U. Seven, and K. Erbatur, "Trajectory generation with natural ZMP references for the biped walking robot SURALP," in *Proc. IEEE Int. Conf. Robot. Autom.*, May 2010, pp. 4237–4242.

[16] Y. Choi, D. Kim, Y. Oh, and B.-J. You, "Posture/walking control for humanoid robot based on kinematic resolution of CoM jacobian with embedded motion," *IEEE Trans. Robot.*, vol. 23, no. 6, pp. 1285–1293, Dec. 2007.

[17] N. Perrin, O. Stasse, L. Baudouin, F. Lamiraux, and E. Yoshida, "Fast humanoid robot collision-free footstep planning using swept volume approximations," *IEEE Trans. Robot.*, vol. 28, no. 2, pp. 427–439, Apr. 2012.

[18] S. Kajita, T. Nagasaki, K. Kaneko, and H. Hirukawa, "ZMP-based biped running control," *IEEE Robot. Autom. Mag.*, vol. 14, no. 2, pp. 63–72, Jun. 2007.

[19] E. Ohashi, T. Sato, and K. Ohnishi, "A walking stabilization method based on environmental modes on each foot for biped robot," *IEEE Trans. Ind. Electron.*, vol. 56, no. 10, pp. 3964–3974, Oct. 2009.

[20] K. Hu, C. Ott, and D. Lee, "Learning and generalization of compensative zero-moment point trajectory for biped walking," *IEEE Trans. Robot.*, vol. 32, no. 3, pp. 717–725, Jun. 2016.

[21] Y.-D. Hong, B.-J. Lee, and J.-H. Kim, "Command state-based modifiable walking pattern generation on an inclined plane in pitch and roll directions for humanoid robots," *IEEE/ASME Trans. Mechatronics*, vol. 16, no. 4, pp. 783–789, Aug. 2011.

[22] Y.-D. Hong, C.-S. Park, and J.-H. Kim, "Stable bipedal walking with a vertical center-of-mass motion by an evolutionary optimized central pattern generator," *IEEE Trans. Ind. Electron.*, vol. 61, no. 5, pp. 2346–2355, May 2014.

[23] Y.-D. Hong and J.-H. Kim, "3-D command state-based modifiable bipedal walking on uneven terrain," *IEEE/ASME Trans. Mechatronics*, vol. 18, no. 2, pp. 657–663, Apr. 2013.

[24] Y.-F. Ho, T.-H. S. Li, P.-H. Kuo, and Y.-T. Ye, "Parameterized gait pattern generator based on linear inverted pendulum model with natural ZMP references," *Knowl. Eng. Rev.*, 2016. [Online]. Available: https://doi.org/10.1017/S0269888916000138

[25] Z. Yu *et al.*, "Gait planning of omnidirectional walk on inclined ground for biped robots," *IEEE Trans. Syst., Man, Cybern. Syst.*, vol. 46, no. 7, pp. 888–897, Jul. 2016.

[26] K. Van Heerden, "Real-time variable center of mass height trajectory planning for humanoids robots," *IEEE J. Robot. Autom. Lett.*, vol. 2, no. 1, pp. 135–142, Jan. 2017.

[27] K. Erbatur and O. Kurt, "Humanoid walking robot control with natural ZMP references," in *Proc. IEEE 32nd Annu. Conf. Ind. Electron. (IECON)*, Nov. 2006, pp. 4100–4106.

[28] K. Erbatur and O. Kurt, "Natural ZMP trajectories for biped robot reference generation," *IEEE Trans. Ind. Electron.*, vol. 56, no. 3, pp. 835–845, Mar. 2009.

[29] R. W. Hamming, "'Lanczos' σ factors and the σ factors in the general case," in *Numerical Methods for Scientists and Engineers*, 2nd ed. New York, NY, USA: Dover, 1986, pp. 534–536.

[30] B. J. Lee, D. Stonier, Y. D. Kim, J. K. Yoo, and J. H. Kim, "Modifiable walking pattern of a humanoid robot by using allowable ZMP variation," *IEEE Trans. Robot.*, vol. 24, no. 4, pp. 917–925, Aug. 2008.

[31] H.-K. Shin and B. K. Kim, "Energy-efficient gait planning and control for biped robots utilizing the allowable ZMP region," *IEEE Trans. Robot.*, vol. 30, no. 4, pp. 986–993, Aug. 2014.

[32] J. H. Park and K. D. Kim, "Biped robot walking using gravity-compensated inverted pendulum mode and computed torque control," in *Proc. IEEE Int. Conf. Robot. Autom.*, vol. 4. May 1998, pp. 3528–3533.

[33] K. Erbatur and U. Seven, "An inverted pendulum based approach to biped trajectory generation with swing leg dynamics," in *Proc. 7th IEEE-RAS Int. Conf. Humanoid Robots*, Nov. 2007, pp. 216–221.

[34] T. Buschmann, S. Lohmeier, M. Bachmayer, H. Ulbrich, and F. Pfeiffer, "A collocation method for real-time walking pattern generation," in *Proc. 7th IEEE-RAS Int. Conf. Humanoid Robots*, Nov. 2007, pp. 1–6.

[35] B. Stephens, "Integral control of humanoid balance," in *Proc. IEEE/RSJ Int. Conf. Intell. Robots Syst. (IROS)*, Oct. 2007, pp. 4020–4027.

[36] T.-H. S. Li *et al.*, "Robots that think fast and slow: An example of throwing the ball into the basket," *IEEE Access*, vol. 4, pp. 5052–5064, 2016.

[37] O. Michel, "Webots^{TM}: Professional mobile robot simulation," *Int. J. Adv. Robot. Syst.*, vol. 1, no. 1, pp. 39–42, Mar. 2004.

TZUU-HSENG S. LI (S'85–M'90) received the B.S. degree in electrical engineering from Tatung Institute of Commerce and Technology, Taipei, Taiwan, in 1981, and the M.S. and Ph.D. degrees in electrical engineering from National Cheng Kung University (NCKU), Tainan, Taiwan, in 1985 and 1989, respectively.

From 1996 to 2009, he was a Researcher with the Engineering and Technology Promotion Center, National Science Council, Tainan. From 1999 to 2002, he was the Director of the Electrical Laboratories, NCKU. From 2009 to 2012, he was the Dean of the College of Electrical Engineering and Computer Science, National United University, Miaoli, Taiwan. Since 1985, he has been with the Department of Electrical Engineering, NCKU, where he is currently a Distinguished Professor. He has been the Director of the Center for Intelligent Robotics and Automation, NCKU, since 2014. His current research interests include artificial and/or biological intelligence and applications, fuzzy system and control, home service robots, humanoid robots, mechatronics, 4WIS4WID vehicles, and singular perturbation methodology.

Dr. Li received the Outstanding Automatic Control Award from the Chinese Automatic Control Society (CACS), Taiwan, in 2006. He was a Technical Editor of the IEEE TRANSACTIONS ON MECHATRONICS, the ASME Transactions on Mechatronics and an Associate Editor of the *Asian Journal of Control*. He is currently an Associate Editor of the *International Journal of Electrical Engineering*, the *International Journal of Fuzzy Systems*, and the IEEE TRANSACTIONS ON CYBERNETICS. He was elected as the President of the CACS from 2008 to 2011, and the Robotics Society of Taiwan from 2012 to 2015. He has been the Vice President of the Federation of International Robot-Soccer Association, since 2009. In 2008, he became a CACS Fellow.

YA-FANG HO was born in Kaohsiung, Taiwan, in 1988. She received the B.S. and the M.S. degrees from the Department of Electrical Engineering, National Cheng Kung University, Tainan, Taiwan, in 2010 and 2011, respectively, where she is currently pursuing the Ph.D. degree with the Department of Electrical Engineering. Her major research interests include fuzzy control, intelligent system, humanoid robot, image processing, robotic application, and FIRA/RoboCup games.

PING-HUAN KUO was born in Pingtung, Taiwan, in 1986. He received the B.S., M.S., and Ph.D. degrees from the Department of Electrical Engineering, National Cheng Kung University, Tainan, Taiwan, in 2008, 2010, and 2015, respectively. His major research interests include fuzzy control, intelligent algorithms, humanoid robot, image processing, and robotic application.

YAN-TING YE received the B.S. and the M.S. degrees from the Department of Electrical Engineering from National Cheng Kung University, Tainan, Taiwan, in 2013 and 2015, respectively. His major research interests include fuzzy control, intelligent system, humanoid robot, image processing, robotic application, and FIRA/RoboCup games.

LI-FAN WU received the B.S. degree from the Department of Mechanical Engineering, National Cheng Kung University, Tainan, Taiwan, in 2015, where he is currently pursuing the M.S. degree with the Department of Electrical Engineering. His major research interests include fuzzy control, intelligent system, humanoid robot, image processing, robotic application, and FIRA/RoboCup games.